

Technical University of Denmark



An Exploratory Flow Reactor Study of H₂S Oxidation at 30-100 Bar

Song, Yu; Hashemi, Hamid; Christensen, Jakob Munkholt; Zou, Chun; Haynes, Brian S.; Marshall, Paul; Glarborg, Peter

Published in:
International Journal of Chemical Kinetics

Link to article, DOI:
[10.1002/kin.21055](https://doi.org/10.1002/kin.21055)

Publication date:
2016

Document Version
Peer reviewed version

[Link back to DTU Orbit](#)

Citation (APA):
Song, Y., Hashemi, H., Christensen, J. M., Zou, C., Haynes, B. S., Marshall, P., & Glarborg, P. (2016). An Exploratory Flow Reactor Study of H₂S Oxidation at 30-100 Bar. *International Journal of Chemical Kinetics*, 49(1), 37-52. DOI: 10.1002/kin.21055

DTU Library

Technical Information Center of Denmark

General rights

Copyright and moral rights for the publications made accessible in the public portal are retained by the authors and/or other copyright owners and it is a condition of accessing publications that users recognise and abide by the legal requirements associated with these rights.

- Users may download and print one copy of any publication from the public portal for the purpose of private study or research.
- You may not further distribute the material or use it for any profit-making activity or commercial gain
- You may freely distribute the URL identifying the publication in the public portal

If you believe that this document breaches copyright please contact us providing details, and we will remove access to the work immediately and investigate your claim.

An Exploratory Flow Reactor Study of H₂S Oxidation at 30–100 Bar

YU SONG,^{1,2} HAMID HASHEMI,¹ JAKOB MUNKHOLT CHRISTENSEN,¹ CHUN ZOU,² BRIAN S. HAYNES,³ PAUL MARSHALL,⁴ PETER GLARBORG¹

¹Department of Chemical and Biochemical Engineering, Technical University of Denmark, DK-2800 Kgs. Lyngby, Denmark

²State Key Laboratory of Coal Combustion, Huazhong University of Science and Technology, Wuhan, 430074, People's Republic of China

³School of Chemical and Biomolecular Engineering, University of Sydney, Sydney, Australia

⁴Department of Chemistry and Center for Advanced Scientific Computing and Modeling (CASCaM), University of North Texas, Denton, TX, 76203-5017

Received 4 July 2016; revised 30 September 2016; accepted 1 October 2016

DOI 10.1002/kin.21055

Published online 9 November 2016 in Wiley Online Library (wileyonlinelibrary.com).

ABSTRACT: Hydrogen sulfide oxidation experiments were conducted in O₂/N₂ at high pressure (30 and 100 bar) under oxidizing and stoichiometric conditions. Temperatures ranged from 450 to 925 K, with residence times of 3–20 s. Under stoichiometric conditions, the oxidation of H₂S was initiated at 600 K and almost completed at 900 K. Under oxidizing conditions, the onset temperature for reaction was 500–550 K, depending on pressure and residence time, with full oxidization to SO₂ at 550–600 K. Similar results were obtained in quartz and alumina tubes, indicating little influence of surface chemistry. The data were interpreted in terms of a detailed chemical kinetic model. The rate constants for selected reactions, including SH + O₂ ⇌ SO₂ + H, were determined from ab initio calculations. Modeling predictions generally overpredicted the temperature for onset of reaction. Calculations were sensitive to reactions of the comparatively unreactive SH radical. Under stoichiometric conditions, the oxidation rate was mostly controlled by the SH + SH branching ratio to form H₂S + S (promoting reaction) and HSSH (terminating). Further work is desirable on the SH + SH recombination and on subsequent reactions in the S₂ subset of the mechanism. Under oxidizing conditions, a high O₂ concentration (augmented by the high pressure) causes the termolecular reaction SH + O₂ + O₂ → HSO + O₃ to become the major consumption step for SH, according to the model. Consequently, calculations become very sensitive to the rate constant and product channels for the H₂S + O₃ reaction, which are currently not well established. © 2016 Wiley Periodicals, Inc. *Int J Chem Kinet* 49: 37–52, 2017

Correspondence to: Peter Glarborg; e-mail: pgl@kt.dtu.dk.
Supporting Information is available in the online issue at
www.wileyonlinelibrary.com.
© 2016 Wiley Periodicals, Inc.

INTRODUCTION

Hydrogen sulfide (H₂S) is a by-product from cleaning of natural gas and synthesis gas produced from

gasification of coal or biomass, from hydrodesulfurization of light hydrocarbons, and from upgrading heavy oils and coals. It is also released from sulfur-containing fuels during pyrolysis or formed under very reducing conditions in combustion processes. The medium to high-temperature chemistry of H_2S has received attention due to its importance in combustion, in the Claus process, and as a potential hydrogen source [1,2]. The H/S system has been investigated for both H_2S pyrolysis and H_2 sulfidation [3–10]. Despite some remaining uncertainties, available experimental results are described satisfactorily by a detailed reaction mechanism [8].

A wide range of studies have dealt with H_2S conversion in the presence of oxygen. Wilson and Hirst [11] discuss atmospheric oxidation of H_2S , whereas early investigations of oxidation at elevated temperatures were reviewed by Cullis and Mulcahy [12]. Experimental results have been reported for explosion limits and induction times in static reactors [13–17], oxidation in flow reactors [18], induction times in shock tubes for H_2S [19] and $\text{H}_2/\text{H}_2\text{S}$ mixtures [20], flame speeds [21–24], and structures of premixed [25–32] and diffusion flames [33].

Early modeling efforts for H_2S oxidation [19,34] largely had to rely on estimated rate constants for the sulfur subset. More recently, Haynes and coworkers investigated the chemistry of H_2S pyrolysis and oxidation in a series of modeling studies [8,18], supported by ab initio calculations for key reactions [35–39]. The mechanism of Zhou et al. [18] was adopted and slightly revised by Mathieu et al. [20] who studied the impact of H_2S on ignition of H_2 over large pressure (1.6–33 atm) and temperature (1045–1860 K) ranges. Bongartz and Ghoniem [40] used the mechanism of Zhou et al. as a starting mechanism for a more thorough optimization study, using rate constants for 15 reactions in the scheme as parameters when modeling a range of experimental data reported in the literature.

With the exception of the shock tube experiments from Frenklach et al. [19] and Mathieu et al. [20], results for H_2S oxidation at elevated pressures are scarce. The objective of the present study is to obtain experimental results for the oxidation of H_2S at high pressure (30–100 bar) as a function of temperature (600–925 K) and stoichiometry (lean to stoichiometric) and analyze them in terms of a detailed chemical kinetic model, based on the work of Zhou et al. [18].

EXPERIMENTAL

The experimental setup was a laboratory-scale high-pressure laminar flow reactor designed to approxi-

mate plug flow. The setup is described in detail elsewhere [41], and only a brief description is provided here. The system was used here for investigation of hydrogen sulfide oxidation at 30 bar and 100 bar pressure, respectively, and temperatures from 450 to 900 K.

The reactions took place in a tubular quartz reactor (inner diameter of 7.5 mm), enclosed in a stainless steel tube that acted as a pressure shell. Using a quartz tube and conducting the experiments at high pressure ensured a minimal contribution from heterogeneous reactions at the reactor wall. However, additional experiments were conducted in an alumina tube (Degussit AL23; inner diameter 6 mm) to assess the importance of surface reactions. The steel tube was placed in a tube oven with three individually controlled electrical heating elements that produced an isothermal reaction zone (± 6 K) of 37–47 cm. The temperature profile in the flow reactor was measured by a thermocouple positioned in the void between the quartz/alumina reactor and the steel shell. Results for 30 bar are shown in Fig. 1, whereas the 100-bar profiles are available as the Supporting Information. The system was pressurized from the feed gas cylinders. The reactor pressure was monitored upstream of the reactor by a differential pressure transducer and controlled by a pneumatically actuated pressure-control valve positioned after the reactor. All gases used in the present experiments were high-purity gases or mixtures with certified concentrations. The total flow rate was 2.8 L min^{-1} (STP).

The product analysis was conducted by an online 6890N Agilent Gas Chromatograph (GC-TCD/FID from Agilent Technologies) with an overall relative measurement uncertainty in the range ± 2 –6%.

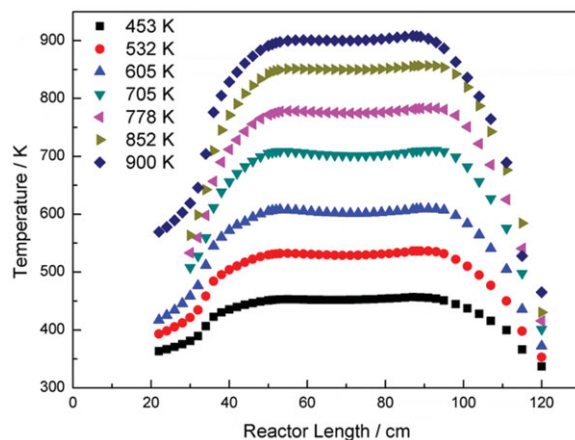


Figure 1 Measured temperature profiles along the reactor axis for 30 bar conditions.

Table I Thermodynamic Properties for Selected Species in the Sulfur Subset. Units are kcal mol⁻¹ for H, and cal mol⁻¹ K⁻¹ for S and C_p. The temperatures for C_p are in K

Species	ΔH_{f298}	S ₂₉₈	C _{p300}	C _{p400}	C _{p500}	C _{p600}	C _{p800}	C _{p1000}	C _{p1500}	
H ₂ S	-4.92	49.18	8.19	8.52	8.91	9.34	10.20	11.00	12.35	[48]
SH	34.23	46.73	7.74	7.59	7.49	7.46	7.59	7.85	8.34	[18,49]
S	66.19	40.11	5.66	5.57	5.44	5.32	5.21	5.13	5.06	[48]
SO	1.14	53.04	7.22	7.53	7.84	8.10	8.42	8.63	8.97	[48]
SO ₂	-70.93	59.32	9.54	10.37	11.10	11.70	12.50	12.98	13.54	[48]
SO ₃	-94.61	61.30	12.13	13.77	15.07	16.07	17.39	18.16	19.00	[48]
HSO	-5.20	57.75	8.54	9.21	9.91	10.53	11.43	12.08	12.90	[48]
HOS	-1.60	57.31	8.78	9.44	10.03	10.50	11.11	11.58	12.38	[48]
HSOH	-28.52	58.66	10.82	12.25	13.46	14.44	15.84	16.61	17.60	[43]
HOSO	-57.70	67.47	11.87	13.43	14.56	15.37	16.40	17.06	18.09	[50]
HSO ₂	-33.80	63.00	11.94	13.68	14.99	15.98	17.28	18.05	18.98	[50]
HSOO	32.29	67.63	12.38	13.58	14.48	15.16	16.10	16.78	17.74	[38]
S ₂	30.73	54.52	7.78	8.14	8.39	8.57	8.77	8.94	9.33	[48]
HSS	25.84	60.94	9.62	10.30	10.80	11.19	11.80	12.26	12.98	[8,36]
HSSH	3.70	61.61	11.63	12.90	13.83	14.57	15.72	16.62	18.02	[8,36]

The plug flow assumption was shown by Rasmussen et al. [41] to be a good approximation for the present operating conditions. The uncertainty in the gas temperature due to the effect of heat release from combustion was limited by a high level of dilution.

DETAILED KINETIC MODEL

The detailed chemical kinetic model for H₂S oxidation was adopted mostly from the recent study on H₂S oxidation by Zhou et al. [18]. The reaction mechanism consists of a H₂ subset [42] and a full description of the H/S/O reaction system [8,18,43–47].

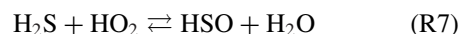
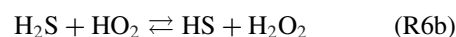
Table I shows thermodynamic properties of selected species. Most of the data are drawn from the database of Goos et al. [48]. The heats of formation of key species such as SH, HSO, and HOS are in agreement within the uncertainty with recent high-accuracy theoretical results [51–53].

Selected reactions from the sulfur subset are listed in Table II. Below selected reactions are discussed in some detail, with emphasis on steps that may have a particular significance under the high-pressure conditions of the present study.

Most of the reactions of H₂S with the radical pool have been characterized experimentally and theoretically over a wider temperature range. For H₂S + H (R2), H₂S + O (R3, R4), and H₂S + S (R12), we rely on rate constants determined by Marshall and coworkers [54,55,58]. The rate constant for H₂S + OH (R5) was taken from the theoretical study by Elling-

son and Truhlar [56]; it provides an explanation for the unusual temperature dependence of the reaction, and the calculated value is in good agreement with experiment [64–68]. The H₂S + O reaction has two product channels, SH + OH (R3) and HSO + H (R4). The branching fraction $k_4/(k_3 + k_4)$ calculated by Goumri et al. [55] agrees with the reported low-temperature upper limit by Singleton and Cvetanovic [69] and, within the uncertainty, with the high-temperature determination by Tsuchiya et al. [70].

Other consumption steps for H₂S have not been characterized experimentally. For the reaction of H₂S with HO₂,



only a room temperature upper limit has been reported [71]. We have adopted the values for k_6 and k_7 , calculated from transition state theory by Zhou et al. [18]. The rate constants for H₂S with O₂ and SO₂ were also drawn from theoretical work of Haynes and coworkers [18,35,36]. For H₂S + O₂, we considered in the present work also the spin-forbidden formation of singlet H₂SOO peroxide, followed by the barrierless decomposition path to HSO + OH identified by Montoya et al. [35]. However, the reaction barrier for the initial step is too high for it to be important under the current conditions. Another possibility, as suggested by Starik et al. [72], is that reaction of H₂S with the tiny equilibrium population of singlet oxygen may promote

Table II Selected Reactions from the H₂S Subset. Parameters for use in the Modified Arrhenius Expression $k = AT^\beta \exp(-E/RT)$. Units are mol, cm, s, cal

		<i>A</i>	β	<i>E</i>	Source
1.	H ₂ S + M \rightleftharpoons S + H ₂ + M	1.6E24	-2.613	89,100	[5]
2.	H ₂ S + H \rightleftharpoons SH + H ₂	3.5E07	1.940	904	[54]
3.	H ₂ S + O \rightleftharpoons SH + OH	7.5E07	1.750	2,900	[55]
4.	H ₂ S + O \rightleftharpoons HSO + H	1.4E09	1.100	5,099	[55]
5.	H ₂ S + OH \rightleftharpoons SH + H ₂ O	8.7E13	-0.700	0	[56] ^a
		4.1E07	1.770	0	
6.	SH + H ₂ O ₂ \rightleftharpoons H ₂ S + HO ₂	5.6E04	2.823	8,668	[18] ^b
7.	H ₂ S + HO ₂ \rightleftharpoons HSO + H ₂ O	1.0E00	3.288	6,224	[18] ^b
8.	SH + HO ₂ \rightleftharpoons H ₂ S + O ₂	3.8E04	2.775	-1,529	[18] ^b
9.	H ₂ S + O ₂ \rightleftharpoons HSO + OH	1.0E11	0.000	49,100	[18] est
10.	H ₂ S + O ₃ \rightleftharpoons SO ₂ + H ₂ O	5.3E08	1.660	11,665	[57]
11.	H ₂ S + O ₃ \rightleftharpoons HOSO + OH	1.1E03	2.770	11,369	[57]
12.	H ₂ S + S \rightleftharpoons SH + SH	7.4E06	2.300	9,007	[58] ^{a,c}
		4.7E07	1.325	-436	[58] ^d
13.	H ₂ S + SO \rightleftharpoons SH + HSO	5.4E03	3.209	26,824	[18] ^b
14.	H ₂ S + SO \rightleftharpoons SH + HOS	1.0E13	0.000	36,500	[18] est
15.	H ₂ S + SO ₂ \rightleftharpoons S ₂ O + H ₂ O	1.7E06	1.857	37,740	[36]
16.	S + H + M \rightleftharpoons HS + M	6.2E16	-0.600	0	[8] est
17.	S + H ₂ \rightleftharpoons SH + H	1.4E14	0.000	19,300	[5]
18.	SH + O \rightleftharpoons SO + H	4.3E11	0.724	-1,027	[37]
19.	SH + O \rightleftharpoons S + OH	1.8E12	0.000	0	[37] ^a
		4.3E06	2.103	3,583	
20.	SH + OH \rightleftharpoons S + H ₂ O	1.0E14	0.000	0	pw, est
21.	SH + OH \rightleftharpoons HOS + H	1.0E13	0.000	7,400	[18] est
22.	SH + HO ₂ \rightleftharpoons HSO + OH	2.5E08	1.477	-2,169	[18] ^b
23.	SH + HO ₂ \rightleftharpoons SO + H ₂ O	3.2E02	2.579	-2,071	[18] ^b
24.	S + H ₂ O ₂ \rightleftharpoons SH + HO ₂	4.1E06	2.200	12,619	[18] ^b
25.	SH + O ₂ \rightleftharpoons HSO + O	2.3E06	1.816	20,008	[38]
26.	SH + O ₂ \rightleftharpoons S + HO ₂	4.7E06	2.017	36,913	[38]
27.	SH + O ₂ \rightleftharpoons SO + OH	7.5E04	2.052	16,384	[38]
28.	SH + O ₂ \rightleftharpoons SO ₂ + H	1.5E05	2.123	11,020	pw
29.	SH + O ₂ (+M) \rightleftharpoons HSOO(+M)	8.7E14	-0.260	298	[50]
	Low pressure limit	3.1E19	-0.201	20	
30.	SH + O ₃ \rightleftharpoons HSO + O ₂	5.7E12	0.000	556	[59]
31.	SH + H ₂ O ₂ \rightleftharpoons HSOH + OH	9.5E03	2.800	9,829	[18] ^b
32.	S + OH \rightleftharpoons SO + H	1.5E13	0.191	-1,361	[37]
33.	S + HO ₂ \rightleftharpoons SO + OH	5.7E13	0.000	0	[60]
34.	S + O ₂ \rightleftharpoons SO + O	5.4E05	2.110	-1,450	[61]
35.	SO + HO ₂ \rightleftharpoons SO ₂ + OH	1.0E12	0.000	0	pw ^e
36.	SO + O ₂ \rightleftharpoons SO ₂ + O	7.6E03	2.370	2,970	[62]
37.	HSO + O ₂ \rightleftharpoons SO + HO ₂	6.4E05	2.627	19,013	[18] ^a
		2.9E01	3.200	14,529	pw ^f
38.	HSO + O ₂ \rightleftharpoons SO ₂ + OH	3.7E01	2.764	6,575	[18]
39.	HSO + O ₂ \rightleftharpoons HSO ₂ + O	8.4E-07	5.100	11,312	[18]
40.	HSO + O ₃ \rightleftharpoons SH + O ₂ + O ₂	1.5E12	0.000	2,230	[59,63]
41.	HSO + O ₃ \rightleftharpoons HSO ₂ + O ₂	1.3E12	0.000	2,230	[59,63]
42.	HSO + O ₃ \rightleftharpoons SO + OH + O ₂	5.0E00	3.630	7,191	pw
43.	SH + SH(+M) \rightleftharpoons HSSH(+M)	9.0E11	0.155	-1,432	[39] ^g
	Low pressure limit:	2.3E31	-4.943	1,998	
	Trope parameters: 1.0 254 2373				
44.	H ₂ S + S(+M) \rightleftharpoons HSSH(+M)	6.4E07	1.280	-478	[39]
	Low pressure limit:	2.4E21	-1.612	1,670	

Continued

Table II Continued

		<i>A</i>	<i>β</i>	<i>E</i>	Source
Troe parameters: 0.5 726 726					
45.	HSSH + SH ⇌ HSS + H ₂ S	6.4E03	2.980	−1,480	[8]
46.	HSS + H ⇌ H ₂ S + S	1.5E08	1.551	2,259	[39] ^a
		4.2E18	−1.563	472	
46.	HSS + H ⇌ SH + SH	9.7E07	1.620	−1,030	[8,39] ^a
		1.6E18	−0.983	261	
47.	HSS + O ₂ ⇌ S ₂ + HO ₂	8.4E01	2.950	7,071	pw
48.	HSS + O ₂ ⇌ HSO + SO	6.6E03	1.900	7,071	pw
49.	HSS + SH ⇌ S ₂ + H ₂ S	6.3E03	3.050	−1,105	[8]

^aDuplicate reaction – the resulting rate constant is the sum of the two expressions.

^bCalculated from TST.

^cAbstraction on the triplet surface.

^dReaction on the singlet surface. Rate constant is the high-pressure limit.

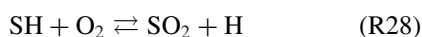
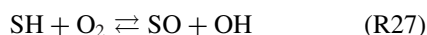
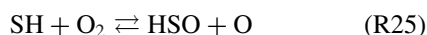
^eReevaluation of the PES indicates that the reaction proceeds without a barrier.

^fThe rate constant for (R37) from Zhou [94] was obtained for quartet transition state. For completeness, we did TST calculations also via the doublet TS.

^gThe high-pressure limit *A* factor was reduced from the value of 3.5E12 calculated by Zhou et al. [39].

the initiation chemistry; however, this was not investigated in the present work.

The reaction of SH with O₂ is a key step in the oxidation of H₂S at high temperature [62]. It has a significant barrier and attempts to measure the rate coefficient at low temperatures have yielded only upper limits, with a value of $2 \times 10^5 \text{ cm}^3 \text{ mol}^{-1} \text{ s}^{-1}$ at 298 K from the study of Stachnik and Molina [73] considered to be the most reliable [59]. The reaction, which has been studied theoretically by a number of groups [38,50,55,74–76], has several proposed product channels:



The theoretical work of Zhou et al. [38] indicated that the reaction proceeds mainly via a four-membered cyclic transition state to form SO + OH (R27) at temperatures below 1000 K, whereas HSO + O (R25) becomes the major product channel above this temperature. However, Garrido et al. [75] identified a new and faster reaction path to form SO₂ + H (R26) via a three-center ring structure.

The existence of the new pathway is supported by the recent theoretical study of Freitas et al. [76]. They characterized a transition state leading from HSOO via an electronically excited state to HSO₂, with a CCSD(T) energy extrapolated to the complete basis set limit of 19.8 kcal mol^{−1} above HSOO. Assuming this is the bottleneck, SH + O₂ collisions will maintain a small equilibrium population of HSOO, which lies 6.4 kcal mol^{−1} below SH + O₂ [77]. Accordingly, we evaluated the bimolecular TST for SH + O₂ → products via this TS with a barrier of 13.4 kcal mol^{−1}. Because HSO₂ is formed with energies *E* of about 82 kcal mol^{−1} or more, well above the S–H dissociation threshold *E*₀ of about 21 kcal mol^{−1} [75], we assume the major products are H + SO₂ (see Table II). We justify this via evaluation of the microcanonical TST result $k(E) = G^\ddagger(E - E_0)/(h N(E))$ for first-order dissociation of nascent vibrationally excited HSO₂. *N*(*E*) is the density of states for HSO₂, and $G^\ddagger(E - E_0)$ is the sum of states for the TS for HSO₂ dissociation to H + SO₂. This yields $k(E) = 1.6 \times 10^{14} \text{ s}^{-1}$, three orders of magnitude faster than collisional stabilization at 100 atm pressure.

Figure 2 shows an Arrhenius plot for the SH + O₂ reaction. Tsuchiya et al. [62] derived the rate constant from measured concentration profiles of H and O atoms in flash-photolysis/shock tube experiments of H₂S/O₂/Ar mixtures. They could not identify the major product channel with certainty, but in their analysis they assumed formation of HSO + O. The theoretical values derived by Zhou et al. [38] and Garrido et al. [75] are all consistent with the room temperature upper limit by Stachnik and Molina [73] but also

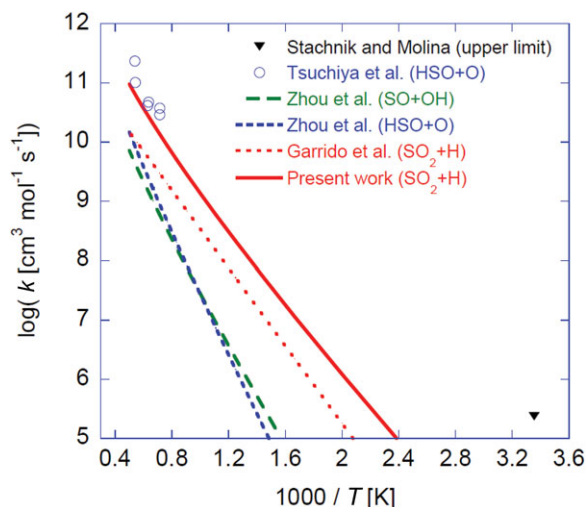


Figure 2 Arrhenius plot for the SH + O₂ reaction. Experimental values are shown as symbols, whereas curves denote rate constants derived from theory. Sources: Stachnik and Molina [73], Tsuchiya et al. [62], Zhou et al. [38], and Garrido et al. [75].

well below the values derived by Tsuchiya et al. The present rate constant for the dominating product channel to SO₂ + H is almost an order of magnitude higher than the value of Garrido et al., used in the modeling study of Zhou et al. [18].

The apparent agreement of the present rate constant with the values of Tsuchiya et al. is fortuitous since they assumed HSO + O to be the major product channel. Actually, Tsuchiya et al. concluded based on their measurements that SO₂ + H was unlikely to be the major product channel for SH + O₂. To resolve this issue, we used the present kinetic model to reinterpret selected data from Tsuchiya et al. (Fig. 3). The comparison shows that the present rate constants and product channels for SH + O₂ are consistent with their measurements. In fact, the present model predictions of H and O show only a limited sensitivity to the rate constant for the SH + O₂ reaction.

At the low to medium temperature, high-pressure conditions of the present work, it is of interest whether an adduct formed from SH + O₂ may have a sufficient lifetime to react. Theoretical studies [38,50,55,75,76] indicate that the thiylperoxyl radical (HSOO) is formed from recombination of SH and O₂,



whereas formation of HSO₂ or HOSO is inaccessible. Turnipseed et al. [78] proposed that reaction (R29) could be partially equilibrated in the atmosphere, with

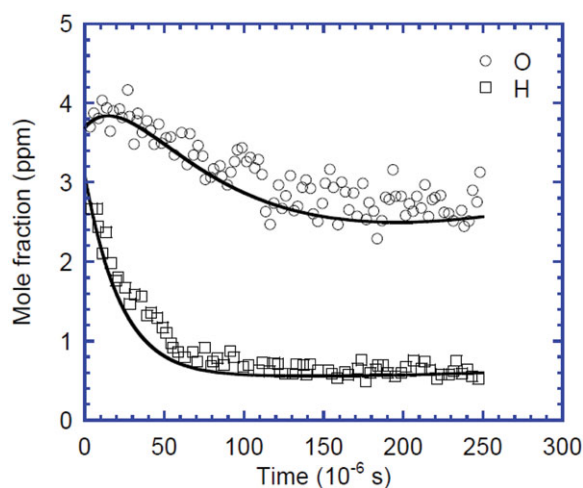
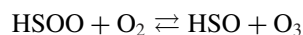


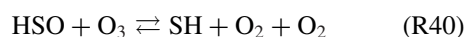
Figure 3 Concentration profiles of O and H atoms after laser photolysis behind a reflected shock wave. Symbols denote experimental results from Tsuchiya et al. [62], whereas curves denote predictions with the chemical kinetic model of the present work. Conditions: $T = 1398$ K, $P = 1.54$ atm, 51 ppm H₂S, 3050 ppm O₂, atomic O and H formed in flash pyrolysis; balance Ar.

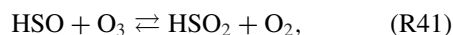
subsequent reactions of with HSOO promoting oxidation of SH. Goumri et al. [50] and Zhou et al. [38] found (R29) to be essentially barrierless, whereas Resende and Ornellas [74] and Ballester and Varandas [79] found barriers of 12 and 8 kcal mol⁻¹, respectively. The difference may partly be attributed to the different geometries of HSOO that are separated by only about 1 kcal mol⁻¹ in energy [75]. The recent study by Garrido et al. [75] calculated a 7 kcal mol⁻¹ barrier to formation of *cis*-HSOO, whereas formation of a skewed HSOO isomer proceeds without a barrier.

The HSOO adduct is weakly bound, and the reaction is rapidly equilibrated. This means that the concentration of HSOO will remain very low, even at the pressures of the present study. Dissociation of HSOO to HSO + O has a significant barrier and is not competitive. However, a fast reaction of HSOO and O₂ (the only abundant reactant under our conditions) could possibly be important,

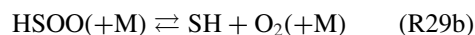
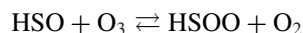


There are no data for this step in the literature, but the reverse reaction, HSO + O₃, has been studied experimentally at low temperatures [63,80–82]. The reaction apparently has two major product channels,





with a branching fraction reported to be roughly 50% at 298 K [59]. Conceivably, the SH + O₂ + O₂ channel (R40) is a sequence of the two steps,



since HSOO decomposes readily even at 298 K. Taking both steps in the reverse direction, we get the sequence $\text{SH} \xrightarrow{+\text{O}_2} \text{HSOO} \xrightarrow{+\text{O}_2} \text{HSO} + \text{O}_3$, which could conceivably be important under the conditions of our work. In the reaction mechanism, we have adopted the one-step reaction (R40), as recommended by Atkinson et al. [59]. However, owing to the fast equilibration of (R29), modeling predictions are not sensitive to whether (R40) is put in as a single reaction or divided into two steps.

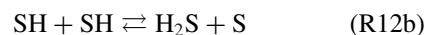
Consequently, SH + O₂ + O₂ → HSO + O₃ (R40b) may be a source of ozone under the conditions of the present work. Ozone is much more reactive than molecular oxygen and may promote reaction. Following other recent studies on low-temperature sulfur chemistry [83,84], we include an O₃ reaction subset with rate constants mostly from Atkinson et al. [59]. Ozone may interact with the O/H radical pool or react with sulfur species, primarily H₂S or SH. The H₂S + O₃ reaction has been studied both experimentally [85–91] and theoretically [57]. Experimental work [88–90] indicates that the overall reaction is complex, involving a radical-forming initial step followed, after an induction time, by a free radical mechanism. Reaction orders of 0–0.5 in H₂S and 1.5 in O₃ have been reported [86,87,89,90]. The reaction appears to be sensitive to surfaces, and reported results show a considerable scatter.

The most reliable measurement of H₂S + O₃ is believed to be the room temperature upper limit by Becker et al. [88]. The recent theoretical study by Mousavipour et al. [57] indicates that SO₂ + H₂O (R10) is the dominating product channel for H₂S + O₃, along with a (very) minor channel forming HOSO + OH (R11). We have tentatively adopted the rate constants from Mousavipour et al., even though the suggestion of (R10) as the dominant channel seems to be inconsistent with the experimental observations.

The rate constant for SH + O₃ (R30) has been measured at low temperature [80,82,92], and values are in good agreement, indicating a fast reaction with a low activation energy. We have adopted the recommendation by Atkinson et al. [59]. The recent theoretical

study by Resende and Ornellas [93] indicates a significantly higher barrier to reaction than derived from experiment. However, this is contradicted by our own preliminary analysis and more work is desirable on this reaction.

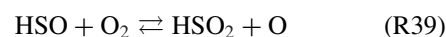
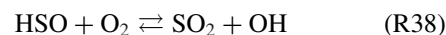
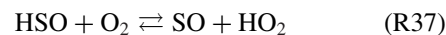
Owing to the low reactivity of the SH radical, the SH + SH reaction becomes important, even at oxidizing conditions. This reaction has two major product channels:



The rate constant for the H₂S + S reaction (R12), which is believed to be largely independent of pressure, was taken from the combined experimental and theoretical study of Gao et al. [58]. The high- and low-pressure limits, as well as the falloff behavior, for the SH + SH recombination step (R43) were initially drawn from the RRKM study of Zhou et al. [39]. However, for this reaction rate parameters are more uncertain, since extrapolation is required. In the present work, we modified the high-pressure limit $k_{43,\infty}$ to improve agreement with experiment under stoichiometric conditions. This is discussed in more detail below. The reaction feeds into the S₂H_x subset, which was drawn largely from Haynes and coworkers [8,39].

Reactions of sulfur radicals with O₂ can be important for the generation of chain carriers, even under conditions with fairly low concentrations of oxygen. In addition to SH + O₂ discussed above, reactions of HSO, SO, S, and HSS with O₂ should be considered. The rate constants for the chain branching steps SO + O₂ and S + O₂ are well established [83,84], but values for HSO + O₂ and HSS + O₂ are more uncertain.

For HSO + O₂, the only reliable measurement is a room temperature upper limit of $1.2 \times 10^7 \text{ cm}^3 \text{ mol}^{-1} \text{ s}^{-1}$ from Lovejoy et al. [81]. The reaction has several possible product channels,



According to theoretical work, the fastest channel is (R38) [18], whereas (R39) is quite slow [46]. However, also (R37) has a significant impact on the system,

Table III Experimental Conditions for the H₂S Oxidation Study

Experiment	Inlet Composition ^{a,b}	Pressure (bar)	Temperature (K)	Residence Time ^c (s)	Reactor
1	756 ppm H ₂ , 1290 ppm O ₂ ; N ₂ ($\phi = 0.88$)	30	450–900	3,520/ <i>T</i> (K)	Quartz
2	750 ppm H ₂ , 1190 ppm O ₂ ; CO ₂ ($\phi = 0.94$)	30	450–900	3,520/ <i>T</i> (K)	Quartz
3	801 ppm H ₂ , 43600 ppm O ₂ ; N ₂ ($\phi = 0.028$)	30	450–900	3,520/ <i>T</i> (K)	Quartz
4	806 ppm H ₂ , 42300 ppm O ₂ ; N ₂ ($\phi = 0.029$)	100	450–900	11,700/ <i>T</i> (K)	Quartz
5	802 ppm H ₂ , 40100 ppm O ₂ ; N ₂ ($\phi = 0.029$)	100	450–900	6,610/ <i>T</i> (K)	Alumina

^aVolume basis; balance N₂ or CO₂.

^bThe fuel air equivalence ratio ϕ is based on the overall reaction H₂S + 1.5O₂ = SO₂ + H₂O.

^cThe nominal residence time in the isothermal region of the reactor. It is a function of temperature, since the mass flow rate was held constant.

because the subsequent reaction of SO with O₂ leads to formation of atomic oxygen.

Prior investigations of HSO chemistry with O₂ relied on G3 energies at CASSCF geometries [94]. Investigation of the HSO + O₂ transition states using CBS-QB3 theory leads to differences in the rate constants of up to a factor of 10. This is consistent with the target energy accuracies of G3 and CBS-QB3 theory for stable species, and we provisionally suggest uncertainties in these reaction barriers of ca. 2.5 kcal mol⁻¹, which corresponds roughly to an order of magnitude in the rate constant.

For HSS + O₂, the original energy calculations were based on MP2/6-31G(d) geometries [18]. We reevaluated the TSs using B3LYP/6-311G(2d,d,p) theory, followed by CBS-QB3 for single-point energies. Based on this, for the doublet TS for HSS + O₂ → HSO + SO, we get a barrier of 39.2 kcal mol⁻¹, and for the two quartet TSs that we attribute to HSS + O₂ → S₂ + HO₂, we get 18.1 and 10.7 kcal mol⁻¹, respectively. In addition, we identified a new doublet TS for HSS + O₂ → S₂ + HO₂ with a barrier of 8.7 kcal mol⁻¹. For this lowest barrier pathway, our TST calculation (including Eckart tunneling and a hindered rotor) yields a rate constant which is about an order of magnitude faster than the previous estimate.

RESULTS AND DISCUSSION

Experiments for H₂S oxidation with high dilution in N₂ (or CO₂) as a function of temperature from 450 to 900 K were conducted under stoichiometric and oxidizing conditions. Table III lists the experimental conditions. The fuel–air equivalence ratio ϕ ranged from 0.9 to 0.03. In the following, the experimental results are compared with modeling predictions. Calculations shown in the figures, conducted using the CHEMKIN PRO software package [95], were restricted to the

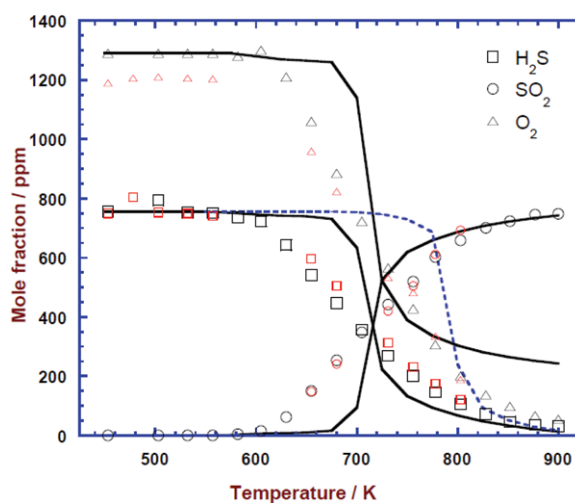


Figure 4 Comparison of experimental data and modeling predictions for H₂S oxidation under stoichiometric conditions at 30 bar. Experimental data are shown as symbols, modeling predictions as solid lines. The dashed line denotes predictions with the original value of $k_{43,\infty}$ (SH + SH (+M) ⇌ HSSH (+M)) from Zhou et al. [39]. Inlet composition: 756 ppm H₂S, 1290 ppm O₂, balance N₂ ($\phi = 0.88$, black symbols) or 750 ppm H₂S, 1190 ppm O₂, balance CO₂ ($\phi = 0.94$, smaller red symbols). The residence time in the isothermal zone is calculated from τ (s) = 3520/*T* (K).

isothermal zone. Simulations with the full measured temperature profile were similar.

Figure 4 shows results for H₂S oxidation under stoichiometric conditions and a pressure of 30 bar with both N₂ and CO₂ as carrier gas. Symbols denote the experimental data, and lines denote numerical results. The onset temperature of the reaction is approximately 625 K. Above this temperature, the degree of conversion increases gradually with temperature; at the highest temperature of 900 K, 30 ppm H₂S and 50 ppm O₂ are still unreacted. The experimental results in CO₂ agree well with those in N₂, showing that the CO₂ has a little effect on the experiment results under these

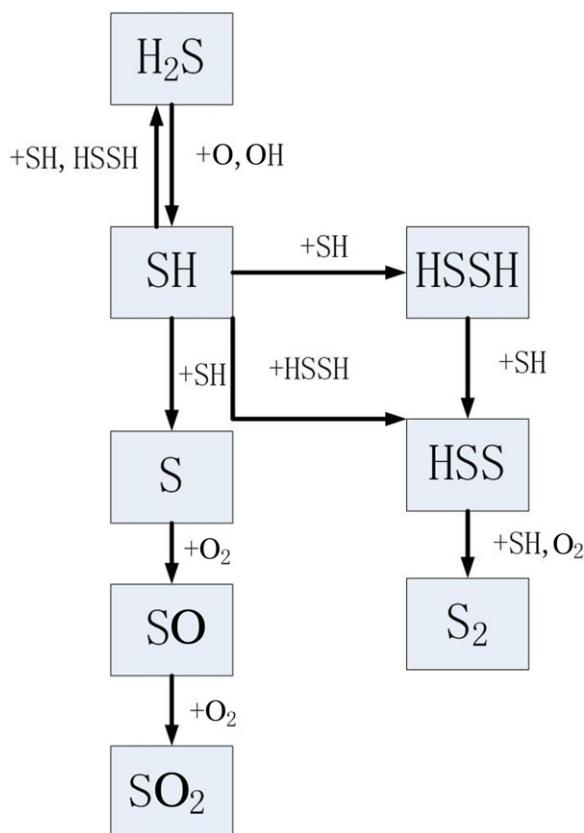


Figure 5 Pathway diagram for H₂S under stoichiometric conditions (corresponding to Fig. 4) and 700 K.

conditions. This is expected, since interaction of CO₂ with the O/H radical pool [96] or with sulfur radicals would be expected to occur only at higher temperatures than those of the present study.

Two sets of modeling predictions are shown. The solid lines denote calculations with the basis mechanism. In this mechanism, we reduced the *A* factor of the high-pressure limit for SH + SH (+M) ⇌ HSSH (+M) (R43) by a factor of four to improve agreement with experiment. This change is considered to be within the uncertainty in the high-pressure limit, for which there are no experimental results. The dashed line shows predictions using the value of $k_{43,\infty}$ calculated by Zhou et al. [39], resulting in a shift upwards in the temperature for onset of reaction of about 100 K.

The modification of $k_{43,\infty}$ allows a satisfactory prediction of the temperature for 50% conversion of H₂S. Still, important differences are seen when comparing experimental results and modeling predictions. Most importantly, the temperature for onset of reaction is overpredicted; the calculations indicate a steeper gradient in the H₂S concentration profile than observed.

Figure 5 shows a reaction path diagram for H₂S oxidation at 700 K and stoichiometric conditions, cor-

responding to Fig. 4. Hydrogen sulfide is consumed by reaction with the O/H radical pool (R3, R5) to form SH. The SH radical is largely consumed by its self-reaction, forming either H₂S + S (R12b) or HSSH (R43). The atomic S is oxidized to SO₂ in the chain-branching sequence S + O₂ → SO + O (R34), SO + O₂ → SO₂ + O (R36). HSSH, on the other hand, is oxidized to S₂ through the sequence HSSH + SH → HSS + H₂S (R45), HSS + SH → S₂ + H₂S (R49), and HSS + O₂ → S₂ + HO₂ (R47). According to the current calculations, formation of oxidized sulfur species from the H_xS₂ is very limited under these conditions.

Figure 6 shows sensitivity coefficients for H₂S under the same conditions (stoichiometric, 700 K). The analysis shows that the predicted H₂S concentration is mainly sensitive to the branching fraction for the SH + SH reaction. Formation of H₂S + S (R12b) strongly promotes the oxidation rate due to the subsequent chain-branching reactions of S and SO with O₂ (R34, R36), whereas formation of HSSH (R43) is chain terminating. None of the reactions in the S₂ subset is seen to promote oxidation; predictions, however, are sensitive to the terminating steps H₂S + S (R44) and HSS + SH (R49). We attribute the discrepancy between experimental results and modeling predictions mostly to uncertainties in the S₂ chemistry.

Figure 7 shows results under oxidizing condition at 30 bar pressure. The initiation temperature is 520 K, approximately 100 K lower than at stoichiometric conditions. Contrary to the behavior in Fig. 4, the concentration gradient of H₂S with respect to temperature is steep and full oxidation to SO₂ is obtained already at 575 K. This indicates that a strong chain-branching mechanism is active already at low temperature.

The model (solid lines) predicts a significantly higher temperature for onset of reaction, about 625 K. However, the concentration profiles are similar to those observed experimentally, just shifted 100 K to higher temperatures. The dashed line shows predictions conducted with the H₂S + O₃ reaction (R10, R11) omitted. Reaction (R10), which is the dominating product channel, serves in effect as a chain-terminating step because it takes out reactive ozone without providing chain carriers. Omission of this step serves to bring the predicted onset temperature in closer accordance with observations. However, this change causes a smaller gradient in H₂S than observed above the onset temperature and leads to an underestimation of SO₂, caused by prediction of significant amounts of SO₃.

Figure 8 shows results under oxidizing condition at 100 bar. The larger black symbols represent experimental results conducted in a quartz tube, whereas the smaller red symbols denote data obtained in an

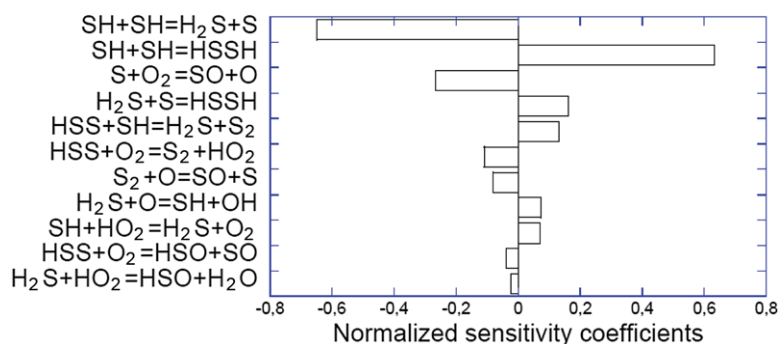


Figure 6 Sensitivity coefficients for H₂S under stoichiometric conditions (corresponding to Fig. 4) and 700 K.

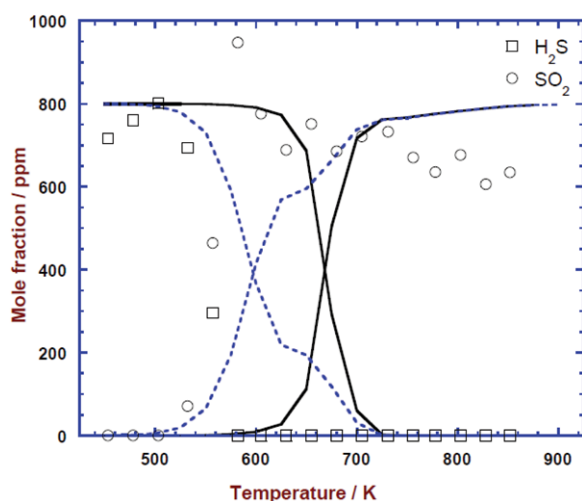


Figure 7 Comparison of experimental data and modeling predictions for H₂S oxidation under oxidizing conditions at 30 bar. Experimental data are shown as symbols, modeling predictions as solid lines. The dashed line denotes predictions omitting the H₂S + O₃ reaction (R10, R11). Inlet composition: 801 ppm H₂S, 4.4% O₂, balance N₂ ($\phi = 0.028$). The residence time in the isothermal zone was τ (s) = 3100/ T (K).

alumina tube. The hydrogen sulfide oxidation is initiated at around 475 K and completed at 550 K. The earlier onset, compared to data at 30 bar, is partly caused by a longer residence time at 100 bar. The behavior is similar to that at 30 bar, except that the initiation temperature is shifted to lower values.

Despite some deviation in residence time, the experimental results from the alumina tube agree well with those of the quartz tube. This is an indication that surface effects, if present, are of minor significance under the conditions with high pressure. This issue is discussed further below.

The modeling results show deviations similar to those at 30 bar. Again, the full model overpredicts

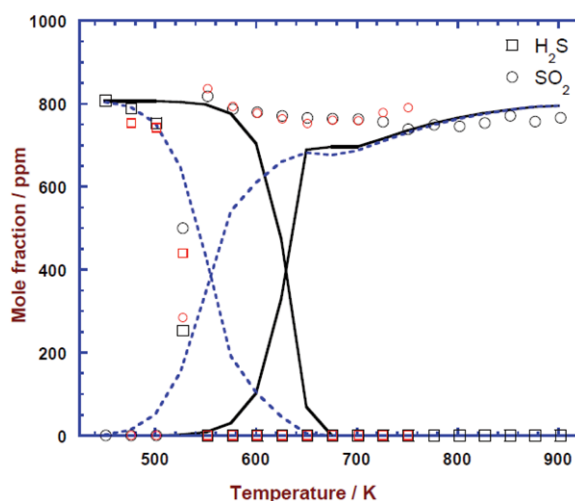


Figure 8 Comparison of experimental data and modeling predictions for H₂S oxidation under oxidizing conditions at 100 bar. Experimental data were obtained in a quartz (black symbols) and an alumina (smaller red symbols) reactor, respectively. Modeling predictions are shown as solid lines. The dashed line denotes predictions omitting the H₂S + O₃ reaction (R10, R11). Inlet composition: 806 ppm H₂S, 4.2% O₂, balance N₂ ($\phi = 0.029$). The residence time in the isothermal zone is calculated from τ (s) = 10,330/ T (K) for the quartz tube and τ (s) = 6610/ T (K) for the alumina tube.

the onset temperature. Omission of (R10) serves to reduce the predicted onset temperature significantly but reduces also the H₂S concentration gradient and the SO₂ level.

Figure 9 shows a reaction path diagram for H₂S oxidation at 600 K and oxidizing conditions, corresponding to Fig. 8. Oxidation paths are very different from those under stoichiometric conditions. A major fraction of the hydrogen sulfide is consumed by reaction with ozone (R10) to form SO₂ directly. A similar amount reacts with O/H radicals (R5, R6b) to form SH, which is consumed by reaction with two oxygen

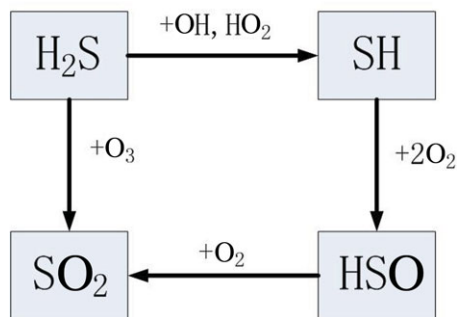


Figure 9 Pathway diagram for H₂S under oxidizing conditions (corresponding to Fig. 8) and 600 K.

molecules (R40b), yielding HSO and O₃. The HSO reacts mostly with O₂ to form SO₂. Owing to the high oxygen concentrations, S₂ species are only formed in minor amounts.

Figure 10 shows sensitivity coefficients for H₂S under lean conditions (100 bar, 600 K). The analysis shows that consumption of H₂S is promoted by chain-propagating or -branching reactions, primarily H₂S + HO₂ (R6b), HSO + O₂ (R38), and H₂S + O (R4). Even though it consumes H₂S, the H₂S + O₃ → SO₂ + H₂O (R10) is a major inhibiting step because it forms stable products. It competes with the minor radical producing channel HOSO + OH (R11), which has a negative sensitivity coefficient.

It is known that oxidation of H₂S is sensitive to surface reactions, and it is important to assess whether heterogeneous effects can explain some of the differences between measurements and modeling predictions under the present conditions. Adesina et al. [9] report that for thermolysis of hydrogen sulfide (i.e., under oxygen-free conditions) there are no indications of surface effects on quartz at 1073 K. However, under oxidizing conditions significant heterogeneous effects have been reported. An increase of the surface to volume ratio

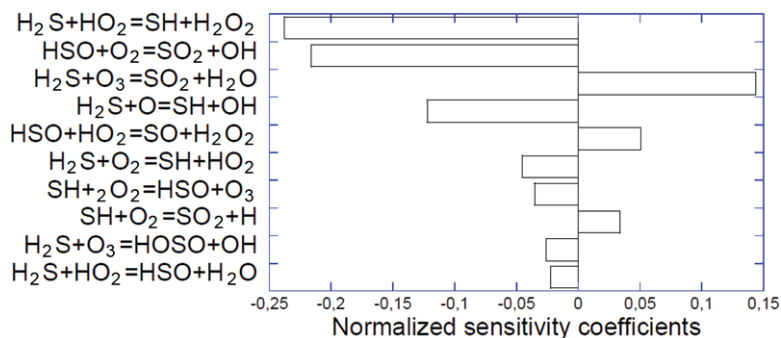


Figure 10 Sensitivity coefficients for H₂S under oxidizing conditions (corresponding to Fig. 8) and 600 K.

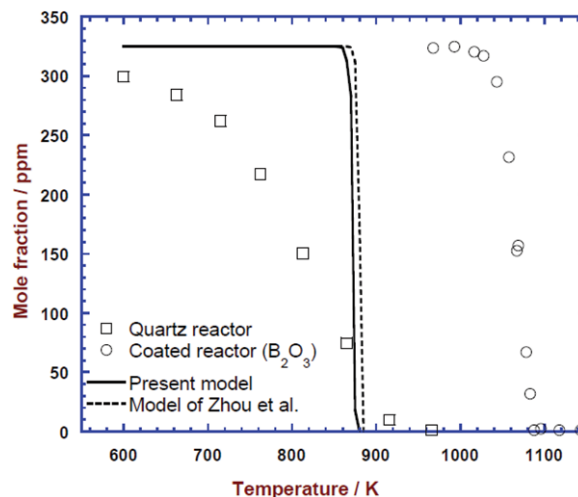


Figure 11 Comparison of modeling predictions for H₂S oxidation with the flow reactor results from Zhou et al. [18]. The experiments were conducted in an uncoated and a coated (B₂O₃) quartz reactor at atmospheric pressure. Inlet composition: 325 ppm H₂S, 600 ppm O₂, balance N₂. The residence time in the isothermal zone was 0.2 s.

in glass reactors serves to inhibit H₂S oxidation and explosion at low pressure and temperatures of 500–600 K [13,14]. Under these conditions, the main impact of the surface seems to be to remove chain carriers, while surface initiation involving a reaction between H₂S and O₂ is less important. More recently, Zhou et al. [18,94,100] investigated the impact of surface effects on H₂S oxidation in quartz flow reactors at atmospheric pressure. They found that a 30-fold increase in the surface area of the reactor slightly enhanced H₂S consumption in the 650–950 K range, while it inhibited formation of H₂ [94,100]. With a B₂O₃ coating of the quartz surface, the system became much less reactive [18,94,100].

Figure 11 compares modeling predictions with the experimental data of Zhou et al. [18], obtained with

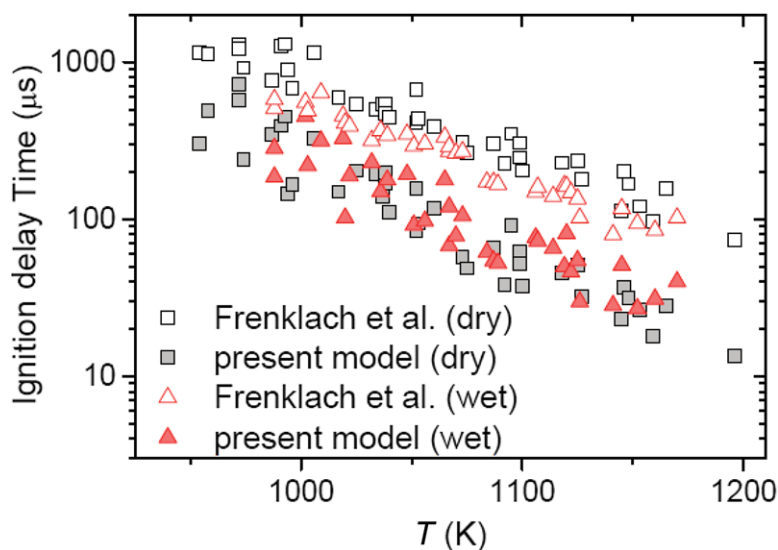


Figure 12 Ignition delay time of $\text{H}_2\text{S}/\text{air}$ (4–22% H_2S , 16–20% O_2) and $\text{H}_2\text{S}/\text{H}_2\text{O}/\text{air}$ (4–21% H_2S , 2–13% H_2O) mixtures versus temperature. Pressure was varied between 29 and 47 atm, whereas the equivalence ratio ϕ changed from 0.3 to 2. Open symbols present experimental data from Frenklach et al. [19], whereas the closed symbols are the results of the present simulations.

and without coating of the quartz reactor surface. The pressure is lower, but the temperature range and composition are comparable to those of the present work. The figure illustrates the considerable impact of the surface condition. Two sets of predictions are shown, conducted with the present model (solid lines) as well as with the basis mechanism of Zhou et al. [18] (dashed lines). Under these conditions, the two mechanisms result in very similar concentration profiles for H_2S . Both models predict the sharp onset of reaction observed in the coated reactor, but the calculated onset temperature is closer to that reported for the uncoated reactor.

Surfaces may initiate reaction and promote oxidation by catalyzing fuel conversion or inhibit oxidation by acting as a sink for radicals. The difference between the impact of the quartz surface between the batch and flow reactor experiments may be attributed to differences in temperature and pressure that could change the balance between surface initiation/oxidation and loss of radicals on the wall. Based on the available results, we believe that the impact of heterogeneous reactions in the high-pressure quartz reactor used in the present work is limited. This is supported by the agreement between results obtained in the quartz and alumina reactors.

To extend the evaluation of the present model, predictions are compared also to selected data obtained at high temperature and pressure in shock tubes. Figure 12 shows data from Frenklach et al. [19] on ig-

nition delays of H_2S in air, with and without presence of water vapor. The experiments were conducted at 34 bar and temperatures in the range 950–1200 K. The present model underestimates the ignition delays by factors of 2–6, most pronounced under dry conditions and at high temperatures.

Figure 13 shows the results of a sensitivity analysis for the ignition delay time under typical conditions (12% H_2S in air, 38 bar, and 1060 K). The sensitivity coefficients are calculated as $(\Delta\tau/\tau)/(\Delta k/k)$, so a negative coefficient indicates a promoting effect. Similar to the flow reactor results, the modeling predictions are very sensitive to the branching fraction for the $\text{SH} + \text{SH}$ reaction. Formation of $\text{H}_2\text{S} + \text{S}$ (R12b) strongly promotes the oxidation rate due to the subsequent chain-branching reactions of S and SO with O_2 (R34, R36) while formation of HSSH (R43) is chain terminating. Also a number of the reactions in the S_2 subset, such as the terminating steps $\text{H}_2\text{S} + \text{S}$ (R44) and $\text{HSS} + \text{SH}$ (R49), show significant sensitivity coefficients. No attempt was made to improve modeling predictions for these conditions; further work is desirable to reduce uncertainties in the S_2 chemistry subset.

Figure 14 compares modeling predictions with ignition delay data from Mathieu et al. [20] for mixtures of H_2 and H_2S , obtained at pressures of about 34 atm and 1045–1860 K. Under these conditions, the radical pool is determined to a larger extent by the H_2/O_2 subset of the mechanism, and the agreement with experiment is better than for the conditions of Frenklach et al.

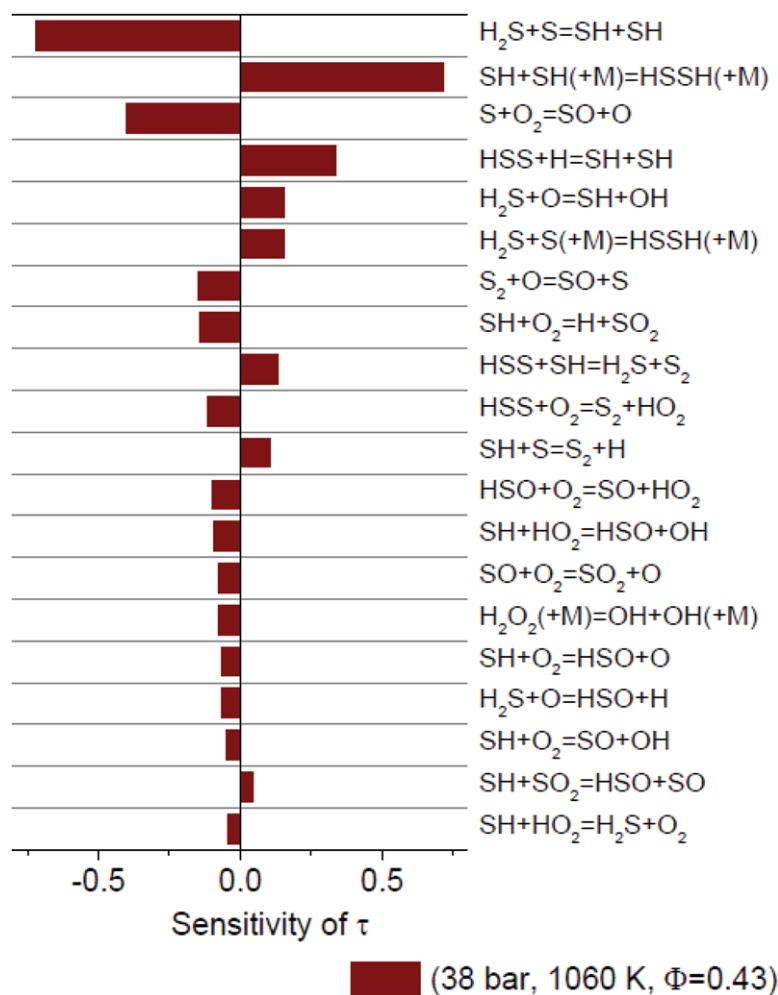


Figure 13 Sensitivity of ignition delay time to the reaction rate constants (corresponding to Fig. 8). Results are shown for 12% H₂S mixed with air ($\phi = 0.43$) at 38 bar and 1060 K.

(Fig. 12). For low concentrations of H₂S (100 and 400 ppm), the predictions compare well to the measurements, but the model systematically underpredicts the ignition delays for higher concentrations of H₂S (1600 ppm).

CONCLUSIONS

Hydrogen sulfide oxidation experiments were conducted at high pressure (30 and 100 bar) under oxidizing and stoichiometric conditions, respectively, and temperatures ranging from 450 to 925 K. The H₂S oxidation behavior depended strongly on the stoichiometry. Under stoichiometric conditions, the oxidation of H₂S was initiated at 600 K, with the consumption rate increasing only slowly with temperature up to 900 K. Under oxidizing conditions, the onset temperature for

reaction was 500–550 K, depending on pressure and residence time, with a steep gradient in H₂S above this temperature. The data were interpreted in terms of a detailed chemical kinetic model. The rate constants for selected reactions, including $\text{SH} + \text{O}_2 \rightleftharpoons \text{SO}_2 + \text{H}$, were determined from ab initio calculations. Modeling predictions generally overpredicted the temperature for onset of reaction. Calculations were sensitive to reactions of the comparatively unreactive SH radical. Under stoichiometric conditions, the oxidation rate was mostly controlled by the SH + SH branching ratio to form H₂S + S (promoting reaction) and HSSH (terminating). Further work is desirable on the SH + SH recombination and on subsequent reactions in the S₂ subset of the mechanism. Under oxidizing conditions, a high O₂ concentration (augmented by the high pressure) causes the reaction $\text{SH} + \text{O}_2 + \text{O}_2 \rightarrow \text{HSO} + \text{O}_3$ to become the major consumption step for SH,

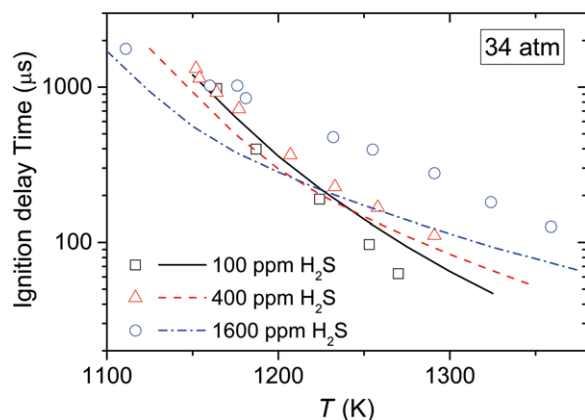


Figure 14 Ignition delay time of $\text{H}_2\text{S}/\text{H}_2/\text{O}_2/\text{Ar}$ mixtures ($\phi = 0.50\text{--}0.58$) versus temperature. The H_2S concentrations are 100, 400, and 1600 ppm, respectively, with 1% H_2 and 1% O_2 . Symbols denote experimental data from Mathieu et al. [20], whereas lines represent simulations conducted at the average pressure of 34.1 atm.

according to the model. Consequently, calculations become very sensitive to the rate constant and product channels for the $\text{H}_2\text{S} + \text{O}_3$ reaction, which are currently not well established.

The work is part of the CHEC (Combustion and Harmful Emission Control) research program at DTU Chemical Engineering. YS wishes to acknowledge funding from CSC (China Scholarship Council). PM thanks the R. A. Welch Foundation (grant B-1174) for support.

BIBLIOGRAPHY

- Raymond, M. E. D. *Hydrocarbon Proc* July, 1975, 139–142.
- Towler, G. P.; Lynn, S. *Ind Eng Chem Res* 1993, 32, 2800–2811.
- Kaloidas, V.; Papayannakos, N. *Chem Eng Sci* 1989, 44, 2493–2500.
- Harvey, W. S.; Davidson, J. H.; Fletcher, E. A. *Ind Eng Chem Res* 1998, 37, 2323–2332.
- Shiina, H.; Miyoshi, A.; Matsui, H. *J Phys Chem A* 1998, 102, 3556–3559.
- Karan, K.; Mehrotra, A. K.; Behic, L. A. *AIChE J* 1999, 45, 383–389.
- Hawboldt, K. A.; Monnery, W. D.; Svrcek, W. Y. *Chem Eng Sci* 2000, 55, 957–966.
- Sendt, K.; Jazbec, M.; Haynes, B. S. *Proc Combust Inst* 2002, 29, 2439–2446.
- Adesina, A. A.; Meeyoo, V.; Foulds, G. *J Hydrogen Energy* 1995, 20, 777–783.
- Binoist, M.; Labégorre, B.; Monnet, F.; Clark, P. D.; Dowling, N. I.; Huang, M.; Archambault, D.; Plasari, E.; Marquaire, P.-M. *Ind Eng Chem Res* 2003, 42, 3943–3951.
- Wilson, C.; Hirst, D. M. *Prog React Kinet* 1996, 21, 69–132.
- Cullis, C. F.; Mulcahy, M. F. R. *Combust Flame* 1972, 18, 225–292.
- Thompson, H. W.; Kelland, N. S. *J Chem Soc* 1931, 1809–1827.
- Farkas, L. *Z Elektrochem* 1931, 37, 670–673.
- Davies, D. A.; Walsh, A. D. *Proc Combust Inst* 1974, 14, 475–483.
- Gray, P.; Sherrington, M. E. *J Chem Soc, Faraday Trans 1* 1974, 70, 2338.
- Pahl, R.; Holtappels, K. *Chem Eng Technol* 2005, 28, 746–749.
- Zhou, C.; Sendt, K.; Haynes, B. S. *Proc Combust Inst* 2013, 34, 625–632.
- Frenklach, M.; Lee, J. H.; White, J. N.; Gardiner, W. C., Jr. *Combust Flame* 1981, 41, 1–16.
- Mathieu, O.; Deguillaume, F.; Petersen, E. L. *Combust Flame* 2014, 161, 23–36.
- Chamberlin, D. S.; Clarke, D. R. *Ind Eng Chem Res* 1928, 20, 1016–1018.
- Cohen, L. *Fuel* 1955, 34, S119–S122.
- Gibbs, G. J.; Calcote, H. F. *J Chem Eng Data* 1959, 4, 226–237.
- Flockenhaus, C. *Gas Wärme Int* 1969, 18, 153–156.
- Levy, A.; Merryman, E. L. *Combust Flame* 1965, 9, 229–240.
- Merryman, E. L.; Levy, A. *J Air Poll Assoc* 1967, 17, 800.
- Sachyan, G. A.; Gershenzon, Yu. M.; Nalbandyan, A. B. *Dokl Akad Nauk SSSR* 1967, 175, 1378.
- Merryman, E. L.; Levy, A. *Proc Combust Inst* 1970, 13, 427–436.
- Selim, H.; Al Shoaibi, A.; Gupta, A. K. *Appl Energy* 2011, 88, 2601–2611.
- Selim, H.; Gupta, A. K.; Al Shoaibi, A. *Appl Energy* 2012, 98, 53–58.
- Selim, H.; Ibrahim, S.; Al Shoaibi, A.; Gupta, A. K. *Appl Energy* 2013, 109, 119–124.
- Selim, H.; Ibrahim, S.; Al Shoaibi, A.; Gupta, A. K. *Appl Energy* 2014, 113, 1134–1140.
- Tesner, P. A.; Rubinov, R. Kh.; Sherov, I. Sh. *Gaz Prom* 1984, 9, 29–30.
- Chernysheva, A. V.; Basevich, V. Ya.; Vedenev, V. I.; Arutyunov, V. S. *Bull Acad Sci USSR* 1991, 39, 1775–1784.
- Montoya, A.; Sendt, K.; Haynes, B. S. *J Phys Chem A* 2005, 109, 1057–1062.
- Sendt, K.; Haynes, B. S. *J. Phys. Chem. A* 2005, 109, 8180–8186.
- Sendt, K.; Haynes, B. S. *Proc Combust Inst* 2007, 31, 257–265.
- Zhou, C.; Sendt, K.; Haynes, B. S. *J Phys Chem A* 2009, 113, 2975–2981.
- Zhou, C.; Sendt, K.; Haynes, B. S. *J Phys Chem A* 2009, 113, 8299–8306.

40. Bongartz, D.; Ghoniem, A. F. *Combust Flame* 2015, 162, 544–553.
41. Rasmussen, C. L.; Hansen, J.; Marshall, P.; Glarborg, P. *Int J Chem Kinet* 2008, 40, 454–480.
42. Hashemi, H.; Christensen, J. M.; Gersen, S.; Glarborg, P. *Proc Combust Inst* 2013, 35, 553–560.
43. Glarborg, P.; Kubel, D.; Dam-Johansen, K.; Chiang, H.-M.; Bozzelli, J. W. *Int J Chem Kinet* 1996, 28, 773–790.
44. Alzueta, M. U.; Bilbao, R.; Glarborg, P. *Combust Flame* 2001, 127, 2234–2251.
45. Dagaut, P.; Lecomte, F.; Mieritz, J.; Glarborg, P. *Int J Chem Kinet* 2003, 35, 564–575.
46. Rasmussen, C. L.; Glarborg, P.; Marshall, P. *Proc Combust Inst* 2007, 31, 339–347.
47. Hindiyarti, L.; Glarborg, P.; Marshall, P. *J Phys Chem A* 2007, 111, 3984–3991.
48. Goos, E.; Burcat, A.; Ruscic, B.; Goos, E.; Burcat, A.; Ruscic, B. *Extended Third Millennium Ideal Gas and Condensed Phase Thermochemical Database for Combustion with updates from Active Thermochemical Tables*, received from Elke Goos, September, 2015.
49. Shiell, R. C.; Hu, X. K.; Hu, Q. J.; Hepburn, J. W. *J Phys Chem A* 2000, 104, 4339–4342.
50. Goumri, A.; Rocha, J.-D. R.; Laakso, D.; Smith, C. E.; Marshall, P. *J Phys Chem A* 1999, 103, 11328–11335.
51. Denis, P. A. *J Sulfur Chem* 2008, 29, 327–352.
52. Nagy, B.; Szakacs, P.; Csontos, J.; Rolik, Z.; Tasi, G.; Kallay, M. *J Phys Chem A* 2011, 115, 7823–7833.
53. Denis, P. A. *Mol Phys* 2010, 108, 1739–1747.
54. Peng, J. P.; Hu, X. H.; Marshall, P. *J Phys Chem A* 1999, 103, 5307–5311.
55. Goumri, A.; Laakso, D.; Rocha, J. D. R.; Smith, C. E.; Marshall, P. *J Chem Phys* 1995, 102, 161–169.
56. Ellingson, B. A.; Truhlar, D. G. *J Am Chem Soc* 2007, 129, 12765–12771.
57. Mousavipour, S. H.; Mortazavi, M.; Hematti, O. *J Phys Chem A* 2013, 117, 6744–6756.
58. Gao, Y.; Zhou, C.; Sendt, K.; Haynes, B. S.; Marshall, P. *Proc Combust Inst* 2011, 33, 459–465.
59. Atkinson, R.; Baulch, D. L.; Cox, R. A.; Crowley, J. N.; Hampson, R. F.; Hynes, R. G.; Jenkin, M. E.; Rossi, M. J.; Troe, J. *Atmos Chem Phys* 2004, 4, 1461–1738.
60. Ballester, M. Y.; Varandas, A. J. C. *Int J Chem Kinet* 2008, 40, 533–540.
61. Lu, C.-W.; Wu, Y.-J.; Lee, Y.-P.; Zhu, R. S.; Lin, M. C. *J Chem Phys* 2004, 121, 8271–8278.
62. Tsuchiya, K.; Kamiya, K.; Matsui, H. *Int J Chem Kinet* 1997, 29, 57–66.
63. Lee, Y.-Y.; Lee, Y.-P.; Wang, N. S. *J Chem Phys* 1994, 100, 387.
64. Westenberg, A. A.; DeHaas, N. *J Chem Phys* 1973, 59, 6685.
65. Perry, R. A.; Atkinson, R.; Pitts, J. N. J. *J Chem Phys* 1976, 64, 3237.
66. Michael, J. V.; Nava, D. F.; Brobst, W. D.; Borkowski, R. P.; Stief, L. J. *J Phys Chem* 1982, 86, 81.
67. Lafage, C.; Pauwels, J.-F.; Carlier, M.; Devolder, P. *J Chem Soc, Faraday Trans 2* 1987, 83, 731.
68. Tyndall, G. S.; Ravishankara, A. R. *Int J Chem Kinet* 1991, 23, 483.
69. Singleton, D. L.; Cvetanovic, R. J. *J Phys Chem Ref Data* 1988, 17, 1377.
70. Tsuchiya, K.; Yokoyama, K.; Matsui, H.; Oya, M.; Dupre, G. *J Phys Chem* 1994, 98, 8419–8423.
71. Mellouki, A.; Ravishankara, A. R. *Int J Chem Kinet* 1994, 26, 355–365.
72. Starik, A. M.; Savelieva, V. A.; Sharipov, A. S.; Titova, N. S. *Combust Flame* 2016, 170, 124–134.
73. Stachnik, R. A.; Molina, M. J. *J Phys Chem* 1987, 91, 4603.
74. Resende, S. M.; Ornellas, F. R. *Phys Chem Chem Phys* 2003, 5, 4617–4621.
75. Garrido, J. D.; Ballester, M. Y.; Orozco-Gonzalez, Y.; Canuto, S. *J Phys Chem A* 2011, 115, 1453–1461.
76. Freitas, G. N.; Garrido, J. D.; Ballester, M. Y.; Nascimento, M. A. C. *J Phys Chem A* 2012, 116, 7677–7685.
77. Grant, D. J.; Dixon, D. A.; Francisco, J. S.; Feller, D.; Peterson, K. A. *J Phys Chem A* 2009, 113, 11343–11353.
78. Turnipseed, A. A.; Barone, S. B.; Ravishankara, A. R. *J Phys Chem* 1992, 96, 7502–7505.
79. Ballester, M. Y.; Varandas, A. J. C. *Phys Chem Chem Phys* 2005, 7, 2305–2323.
80. Friedl, R. R.; Brune, W. H.; Anderson, J. G. *J Phys Chem* 1985, 89, 5505–5510.
81. Lovejoy, E. R.; Wang, N. S.; Howard, C. J. *J Phys Chem* 1987, 91, 5749–5755.
82. Wang, N. S.; Howard, C. J. *J Phys Chem* 1990, 94, 8787–8794.
83. Glarborg, P.; Marshall, P. *Int J Chem Kinet* 2013, 45, 429–439.
84. Glarborg, P.; Halaburt, B.; Marshall, P.; Guillory, A.; Troe, J.; Thellefsen, M.; Christensen, K. *J Phys Chem A* 2014, 118, 6798–6809.
85. Gregor, I. K.; Martin, R. L. *Aust J Chem* 1961, 14, 462–468.
86. Cadle, R. D.; Ledford, M. *Int J Air Water Pollut* 1966, 10, 25–30.
87. Hales, J. M.; Wilkes, J. O.; York, J. L. *Atmos Environ* 1969, 3, 657–667.
88. Becker, K. H.; Inocencio, M. A.; Schurath, U. *Proc Symp Chem Kinet Data Upper Lower Atmos* 1975, 205–220.
89. Glavas, S.; Toby, S. *J Phys Chem* 1975, 79, 779–782.
90. Glavas, S.; Toby, S. *Am Chem Soc Symp Ser* 1975, 17, 122–131.
91. Larin, I. K.; Spasskii, A. I.; Trofimova, E. M.; Turkin, L. E. *Kinet Catal* 2010, 51, 1–5.
92. Schoenle, G.; Rahman, M. M.; Schindler, R. N. *Ber Bunsenges Phys Chem* 1987, 91, 66–75.
93. Resende, S. M.; Ornellas, F. R. *Chem Phys Lett* 2001, 349, 123–130.

94. Zhou, C. Ph.D. thesis, The University of Sydney, 2009.
95. CHEMKIN PRO version 15131, Reaction Design, San Diego, CA, 2013.
96. Glarborg, P.; Bentzen, L. L. B. *Energy Fuels* 2008, 22, 291–296.
97. Denis, P. A. *Chem Phys Lett* 2004, 395, 12–20.
98. Davidson, F. E.; Clemo, A. R.; Duncan, G. L.; Browlet, R. J.; Hobson, J. H.; Grice, R. *Mol Phys* 1982, 46, 33–40.
99. Balucani, N.; Casavecchia, P.; Stranges, D.; Volpi, G. G. *Chem Phys Lett* 1993, 211, 469–472.
100. Zhou, C.; Sendt, K.; Haynes, B. S. *Proc Aust Combust Symp* 2007, 78–81.